Original research article

Journal of Vibration and Control
2026, Vol. 0(0) 1–18

DOI: 10.1177/10775463261445432
journals.sagepub.com/home/jvc

Bio-inspired irregular lattices as enhanced lightweight dampening system

Ahmad Burhani Ahmad Basri[1], **Ranganayagi Venkatmohan**[1] and **Simone Andresen**[1]

Abstract

Vibration dampers play a crucial role in mitigating high-vibration amplitudes in engineering structures. However, in applications where lightweight and cost-effectiveness are paramount, the use of heavy and expensive dampers as additional components appears counterintuitive. Implementing a low-weight high-damping mechanism in a system will not only help to reduce the amplitude of vibration but also avoid resonance. This paper investigates irregular lattice configurations inspired by diatoms, radiolaria, and glass sponges to serve as lightweight, high-stiffness, and damping mechanisms in a frequency-dependent manner. Lattices featuring regular and irregular shapes with identical weights are designed and manufactured with the selective laser sintering technique using polyamide 12 (PA12) as the material. Finite element analyses and vibration tests in the range of 0–50 Hz are conducted to obtain the measured and numerical damping coefficient, stiffness, and loss factor of each lattice. Subsequently, the results are analysed and compared across different lattice configurations. The comprehensive findings indicate that lattices with higher structural irregularity, quantified using the proposed geometric irregularity index I_{irr}, exhibit improved damping behaviour and stiffness across all studied frequencies. Furthermore, the bio-inspired irregular lattices exhibit a more intricate and frequency-sensitive response while regular lattices exhibit a smoother, monotonous decline in the loss factor and damping coefficient with increasing frequency. In conclusion, this research indicates that incorporating irregular characteristics has a high potential to manipulate the damping behaviour of lightweight lattice structures.

Keywords

bioinspiration, damping, structural irregularities, lattice, vibration, lightweight design

Received: 3 February 2026; accepted: 6 April 2026

1. Introduction

Vibration control is a critical aspect of engineering design to ensure a system's structural integrity and operational performance (Zhu et al., 2024). High-vibration amplitudes can lead to undesirable consequences such as reduced lifespan, increased maintenance costs, and compromised functionality. Furthermore, designing lightweight structures presents an additional challenge for engineers as they are much more prone to vibrate and rattle (Baader and Fontana, 2017; Ljunggren and Ågren, 2002). Regarding beam structures, for example, the trend towards larger and lighter designs has increased the flexibility, which leads to a dense distribution of natural frequencies and intense non-linear behaviour (Chen et al., 2025). Thus, the mitigation of high-vibration amplitudes in lightweight engineering structures stands as a pressing challenge. Classical approaches of vibration suppression are vibration isolation (i.e. avoiding vibrations by blocking their transmission paths) and vibration absorption (i.e. dissipating the vibration energy) (Bai et al., 2025). Both strategies can be active, semi-active, and passive. Undesired vibrations in engineering structures are commonly avoided employing dampers (Lu et al., 2023; Shah et al., 2023; Zhou and Bao, 2025). However, the traditional approach of using (heavy) dampers may not always be feasible, particularly in applications where the lightweight aspect is of paramount importance. As to the prevention of undesired vibrations, non-linear vibrational metamaterials also show a high

[1]Department Bio-inspired Lightweight Design, Bremerhaven, Alfred Wegener Institute Helmholtz Center for Polar and Marine Research (AWI), Germany

Corresponding author:
Simone Andresen, Department Bio-inspired Lightweight Design, Alfred Wegener Institute Helmholtz Center for Polar and Marine Research (AWI), Am Handelshafen 12, Bremerhaven 27570, Germany.
Email: simone.andresen@awi.de

potential for vibration suppression, as reviewed by Bai et al. (2025). One example is quasi-zero-stiffness vibration isolators that contain both strong load-bearing capacity and superior performance in low-frequency vibration isolation based on a lightweight metamaterial (Feng et al., 2026).

With regard to technical lightweight structures, regular structures are commonly utilised such as honeycomb sandwich constructions, lattice frameworks, and steel girders employed in aircrafts, buildings, or cranes due to their excellent mechanical properties (Catchpole-Smith et al., 2019; Do et al., 2020; Han and Lu, 2018; Valdevit et al., 2006). Besides their lightweight potential (Gibson, 1989; Lin et al., 2022), research shows that they exhibit damping capabilities, for example, energy absorption during compression (Evans et al., 2010; Maskery et al., 2017; Ozdemir et al., 2016). Furthermore, regular lattices have also shown the ability to isolate vibration (Azmi et al., 2022; Syam et al., 2018; Yin et al., 2014). Syam et al. (2018) studied different strut-based lattice structures aimed at improving the mechanical vibration isolation of a machine frame while preserving its structural integrity. Their findings revealed that by varying the strut configuration, the vibration isolation capability can be manipulated without compromising the structural integrity. Li et al. (2025) investigated structures based on a combination of truss and plate concluding that the vibration mitigation and energy absorption can be significantly altered by changing the geometric parameters.

Aside from regular structures, irregular forms of lattices have also received significant attention from both industry and research community due to their versatility and the significant improvement in mechanical properties and engineering application over regular lattices. Several studies have revealed that Young's modulus increases significantly with an increase in the irregularity of the cell arrangement of lattice structures (Van der Burg et al., 1997; Zhu et al., 2000, 2001). Okubo et al. (2023) showed that by controlling the level of irregularities in a lattice, a notable improvement in compression resistance can be achieved. Wang et al. (2018) used Voronoi tessellation to design an irregular lattice structure, and through compression tests, discovered that porosity and irregularity significantly affect material properties. Sienkiewicz et al. (2020) investigated gradient lattice structures (unit cell size gradually changed) manufactured with selective laser melting, including discrete, increasing, and decreasing gradient structures, demonstrating their distinct mechanical behaviours compared to regular lattices which are valuable for energy absorption applications.

Apart from technical lightweight cellular structures, biological forms and shapes have long served as a rich source of inspiration for bio-inspired lightweight engineering innovations offering remarkable solutions to complex problems, for example, Ashby and Gibson (1997); Gibson (1985); Seki et al. (2010). Biological lightweight structures like the shells/skeleton of diatoms, radiolaria, or glass sponges (Figure 1), for example, often exhibit a high degree of complexity. The complex and irregular shell patterns and structures of diatoms possess remarkable properties of efficiency, adaptability, and lightweight construction (Adhikari, 2023; Hamm, 2005; Liu and Faisal, 2022; Round et al., 1990). Hamm et al. (2003) showed that significant energy is required to crush the diatom frustule in comparison to their small size which demonstrates their remarkable mechanical properties. More diatom-inspired studies in diverse fields and applications can also be found in, for example, Andresen et al. (2023); Bachir (2024); Breish et al. (2023); D'Mello et al. (2022); Hamm et al. (2015); Heinrichs et al. (2017); Li et al. (2022); Maier et al. (2013); Wee et al. (2005).

Diatom shells protect the inside living organism. A high diversity of diatom shell patterns has evolved in response to different environmental challenges. Regarding the vibration properties of these lightweight shells, it is expected that the structural patterns are also adapted towards vibrational loads, since copepods that feed on diatoms generate vibrations (feeding tools move at rates of 20–80 Hz) to crack open the diatom shell (Koehl and Strickier, 1981).

Different numerical studies have concluded that diatom-inspired irregular structures (2D cellular structures and 3D lattices) and design method observed in diatoms, for example, forming structures according to mode shapes, can significantly manipulate eigenfrequencies, and are a promising approach to design lightweight structures with high eigenfrequencies (Andresen et al., 2020a, 2020b, 2024; Andresen, 2021; Andresen and Ahmad Basri, 2024). Aside from the increased eigenfrequencies of irregular structures compared to regular ones, the introduction of irregular cross-section diameters to lattice struts does also rise eigenfrequencies of 3D irregular (Andresen et al., 2020a) and cubic lattice structures (Cheng et al., 2018).

Despite the abundance of research on regular and irregular lightweight structures, there are only a few comprehensive investigations into the dynamic properties, especially with a focus on damping properties. In a first study on the damping properties of bio-inspired lattices, Andresen et al. (2020a) measured the damping ratio of three different lattices. However, due to the low number of studied lattices, general statements could hardly be made. The damping properties of regular lattice structures have been investigated by Jiangwei et al. (2021); Monkova et al. (2021); Scalzo et al. (2021). While the investigation from Monkova et al. (2021) concluded that the damping behaviour decreases with an increase in eigenfrequency and stiffness, in the other two studies, high-stiffness lattices showed superior damping properties. Jiangwei et al. (2021) studied three irregular (stochastic) lattices with different general cell sizes demonstrating that the damping ratio increases with increasing cell size. Aside from this, recent research lacks detailed investigations on the damping behaviour of irregular lattices. Given that irregular structures can place material in regions where it is most needed to

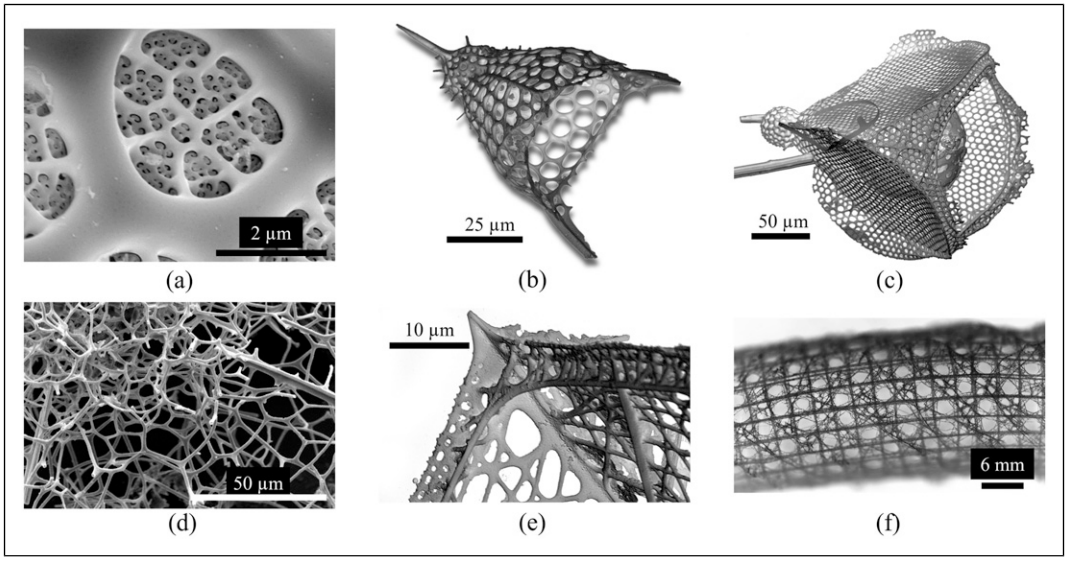

Figure 1. Biological lattice structures observed in scanning electron microscopy images of (a) the diatom *Isthmia* sp., (b–e) different radiolaria, and (f) a glass sponge (all images © AWI).

enhance damping properties, and considering their superior mechanical properties compared to regular lattices, it is anticipated that bio-inspired irregular lattice structures will exhibit improved damping properties.

The presented study aims to explore irregular lattices as lightweight high-stiffness high-damping structures compared to regular lattices. The objective is to show that the studied irregular lattices outperform regular lattices in stiffness and damping properties. Lattice design, additive manufacturing, numerical FRA (frequency response analyses), and vibration experiments were considered in addressing the research question.

2. Materials and methods

In this chapter, the procedure (Figure 2) and methods of the present research are summarised. To investigate the impact of structural irregularities on damping characteristics, two regular and six irregular lattices were designed using the software Synera (Ver. Fabulous Freya, Synera GmbH, Bremen, Germany), which allowed the development of complex biologically inspired lattice structures (e.g. by using field functions to gradually distribute points within a volume that were connected to build the lattice struts, or to define the distribution of the cross-section diameters of the struts). The software HyperMesh and the numerical solver OptiStruct (both Ver. 2019, Altair®HyperWorks®, Altair Engineering, Inc., Troy, Michigan, USA) were utilised to mesh all the structures, create the model setup, solve the FRA, and perform the normal modes analyses. The post-processing of the FRA results was performed using MATLAB (Ver. R2023a, MathWorks, Massachusetts, USA) to obtain the damping coefficient, stiffness, and loss factor. These results were then compared with the experimental data.

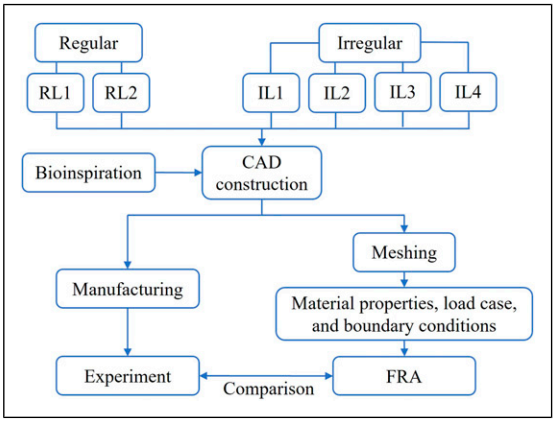

Figure 2. Workflow of the research.

2.1. Lattice structure design and manufacturing

Each lattice structure was designed within the design space illustrated in Figure 3. The dimensions of the design space along the *x*-, *y*-, and *z*-axes were set to 105 mm, 76 mm, and 72 mm, respectively. At the ends of the design space, two rectangular plates were included as the non-design space. These plates, with bore holes, permitted the fixation of the structure to the table and shaker during the experimental test.

Ensuring consistent weight among all lattices was critical so that any differences in damping were only affected by structural adaptations. The six lattices were set to have a constant mass of 0.057 ± 0.001 kg using polyamide (PA12)

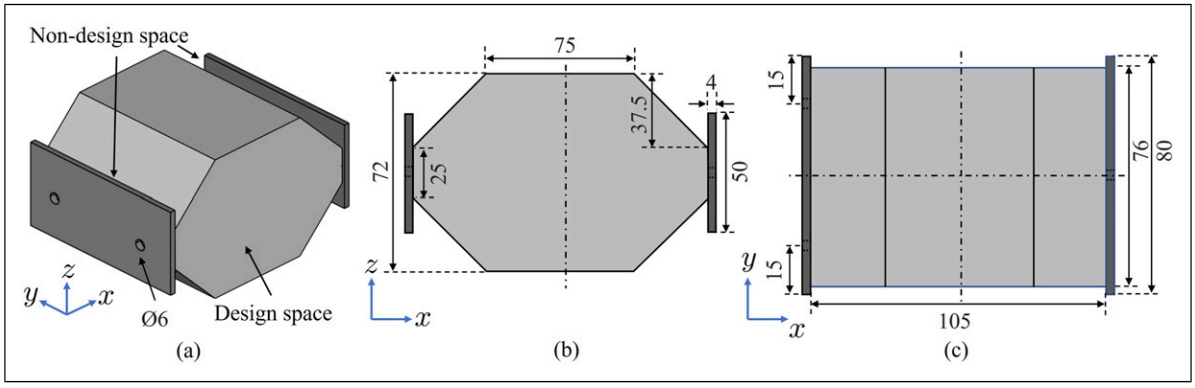

Figure 3. (a) Isometric view, (b) side view, and (c) top view of the design (dark grey) and non-design (light grey) space. The dimensions are given in mm.

as the material. The material properties of PA12 are listed in Table 1.

The lattice structure design has been inspired by diatoms, radiolaria, and glass sponges (Figure 1). In the frame of biomimetics and bioinspiration, the biological role models have previously been studied and their lightweight design principles have been characterised including ribbing structures, hierarchical design structures, irregular strut configuration patterns, and distinct unit cell types. In the present study, the bio-inspired concepts of using regular unit cells, variations in cross-section diameters, and complex irregular strut configurations have been considered.

The lattice structures (see images of the CAD models in the supplemental material) were constructed as follows:

(1) Regular lattice 1 (RL1) was based on a simple cubic unit cell (SCC) pattern. While other unit cell designs such as body-centred cubic and face-centred cubic unit cells were initially considered, practical limitations in available design space and manufacturability led to the preference for SCC for creating the regular lattice. The RL1 was built by a repetition of 6, 6, and 4 SCC unit cells in the x, y, and z directions, respectively. The constant radius of the circular cross-section of the lattice struts was 0.8 mm.
(2) Regular lattice 2 (RL2) was constructed based on the same unit cell as RL1. However, the lattice had only 3, 3, and 2 SCC unit cells in the x, y, and z directions, respectively. The constant radius of the circular cross-section of the lattice struts was 1.412 mm.
(3) Irregular lattice 1 (IL1) showed the same strut layout as RL2. However, the varying strut cross-section diameters gradually increased towards the centre of the lattice. The radius of the struts ranged from 0.800 mm to 1.652 mm.
(4) Irregular lattice 2 (IL2) was based on a random point distribution in which density decreased towards the centre of the lattice. The connection of neighbouring points resulted in the lattice layout. The constant cross-section radius of the struts was 1.155 mm.
(5) Irregular lattice 3 (IL3) was based on a random point distribution having a constant point density, that is, a constant distance between neighbouring points of 36 mm. The uniform radius of the struts' cross-sections was 1.215 mm.
(6) Irregular lattice 4 (IL4) was constructed based on the IL3 layout (see side-by-side comparison shown in the supplemental material), but the cross-section radius of the struts gradually increased towards the lattice centre. The radius of the struts ranged from 0.800 mm to 1.290 mm.

A comprehensive overview of the geometric properties of the lattices is shown in Table 2.

To provide a quantitative indication of structural irregularity, a geometric irregularity index I_{irr} was introduced. The index combines the variation of strut cross-sections, the spread of strut orientations, and variation of point spacing nonuniformity, and is defined as

$$I_{irr} = \frac{r_{max} - r_{min}}{\overline{r}} + \frac{\Theta_{so}}{180^\circ} + \frac{d_{max} - d_{min}}{\overline{d}} \quad (1)$$

$$\overline{r} = \frac{1}{2}(r_{max} + r_{min}) \quad (2)$$

$$\Theta_{so} = \theta_{max} - \theta_{min} \quad (3)$$

Table 1. Defined material properties for polyamide PA12.

Property	Value
Young's modulus E (MPa)	2400
Density ρ (kg m^{-3})	1010
Poisson's ratio ν (–)	0.40
Shear modulus G (MPa)	691.07

Table 2. Geometric properties of the lattices.

Parameters	RL1	RL2	IL1	IL2	IL3	IL4
Number of unit cells in *x*, *y*, *z* direction	6,6,4	3,3,2	3,3,2	—	—	—
Unit cell volume (m^3)	$1.895e^{-6}$	$15.16e^{-6}$	$15.16e^{-6}$	—	—	—
Distance between distributed points (mm)	17.5	35	35	25-31	36	36
Number of joints	350	68	68	72	52	52
Total number of struts	888	147	147	197	156	156
Radius of the circular strut cross-section (mm)	0.800	1.412	0.800–1.652[a]	1.155	1.215	0.800–1.290[a]
Angle between struts (°)	90	90	90	0−180 (random)	0−180 (random)	0–180 (random)
Total mass (kg)	0.05653	0.05745	0.05658	0.05746	0.05782	0.05819

[a]Increasing towards the centre.

$$\overline{d} = \frac{1}{2}(d_{max} + d_{min}) \tag{4}$$

where $r_{\max}$, $r_{\min}$, and $\overline{r}$ denote the maximum, minimum, and mean strut radii, respectively, $\theta_{\max}$ and $\theta_{\min}$ represent the maximum and minimum strut orientation angle in the lattice, Θ_{so} denotes the angular spread of the strut orientations, and $d_{\max}$, $d_{\min}$, and $\overline{d}$ denote the maximum, minimum, and mean point-to-point distance. Thus, the first term characterizes the degree of cross-section nonuniformity, the second term quantifies the variation in strut orientation, and the third term characterizes the spacing nonuniformity between strut connecting points. All terms are normalised to ensure dimensionless consistency. For regular lattices with constant strut radii, orthogonal strut orientations, and uniform point spacing, I_{irr} is zero. Larger values of I_{irr} indicate a higher degree of geometric irregularity arising from cross-section gradients, irregular strut layouts, nonuniform point spacing, or a combination of all. Table 3 shows the calculated I_{irr} for each model. Based on this descriptor, the investigated lattices can be ordered as RL1 = RL2 < IL1 < IL3 < IL2 < IL4 in terms of increasing structural irregularity.

The selective laser sintering (SLS) manufacturing technique was used to manufacture the lattices permitting the formation of complex lattices without the need for support structures. Figure 4 shows the manufactured lattices made from PA12.

Table 3. Geometric irregularity index I_{irr} of the studied lattices.

Model	$\frac{r_{max}-r_{min}}{\overline{r}}$	$\theta_{so}/180°$	$\frac{d_{max}-d_{min}}{\overline{d}}$	I_{irr}
RL1	0.000	0.000	0.000	0.000
RL2	0.000	0.000	0.000	0.000
IL1	0.695	0.000	0.000	0.695
IL2	0.000	1.000	0.214	1.214
IL3	0.000	1.000	0.000	1.000
IL4	0.469	1.000	0.000	1.469

2.2. Experimental analysis

Vibration measurements were conducted at the test laboratory of the Institute of Mechanics, part of the Faculty of Mechanical Engineering at Otto von Guericke University Magdeburg, Germany, to obtain the dissipated energy, maximum strain energy, and displacement amplitude, which subsequently served as the basis for calculating essential damping parameters.

Figure 5 shows the experimental setup. One side of the structure was affixed to an aluminium bar via two M6 bolts. An electrodynamic shaker was used to excite the lattice structures. This excitation mechanism was facilitated by coupling the shaker to the opposite end of the lattice using an M6 bolt, linking it to a stinger along with a force transducer. During experimentation, the force transducer (PCB Piezotronics, Inc.) accurately gauged the shaker's force output. The excitation force was modulated through a power amplifier, ensuring optimal control over the excitation force signal. Meticulous fixation of the shaker to the platform mitigated self-vibration influences.

To measure the lattice displacements, a Laser Doppler Vibrometer (LDV) was directed towards a small aluminium plate affixed to the shaker (see Figure 5(b)). A rig arm was used to hold and fix the LVD position. A reflective tape was adhered to the aluminium plate to reflect the laser beams. The LDV's laser alignment was carefully adjusted, ensuring precise reflection without distortion. Both the force transducer and LDV were interfaced with a data acquisition system.

A single-frequency sine sweep excitation signal was employed with excitation frequencies progressing from 5 Hz to 50 Hz in increments of 5 Hz adhered to a conditioning amplifier limit range of 31.6 mV/unit. When this threshold was reached, the shaker paused momentarily before resuming measurements, safeguarding the integrity of data collection. Each reported data point represents the mean value obtained from approximately 10 steady-state cycles per excitation frequency extracted from the measured time

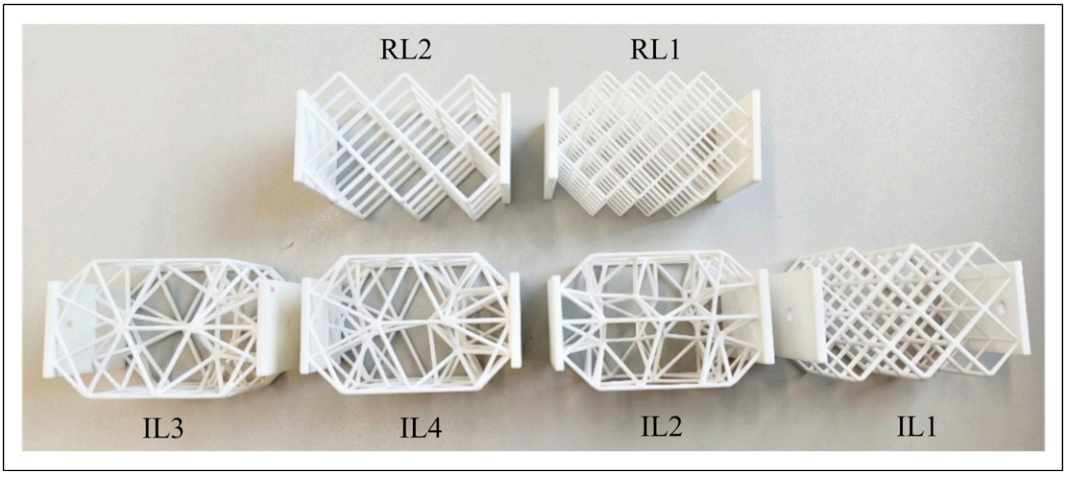

Figure 4. Manufactured lattice structures.

history. The outlined procedure was consistently replicated for each lattice structure. The processed output data from the data acquisition system were subsequently transferred to a computer for visualisation and analytical interpretation.

Critical parameters encompassing the damping coefficient, stiffness, and loss factor were derived from the measured outcomes for each lattice structure (Rao, 2011). The damping coefficient c was computed as

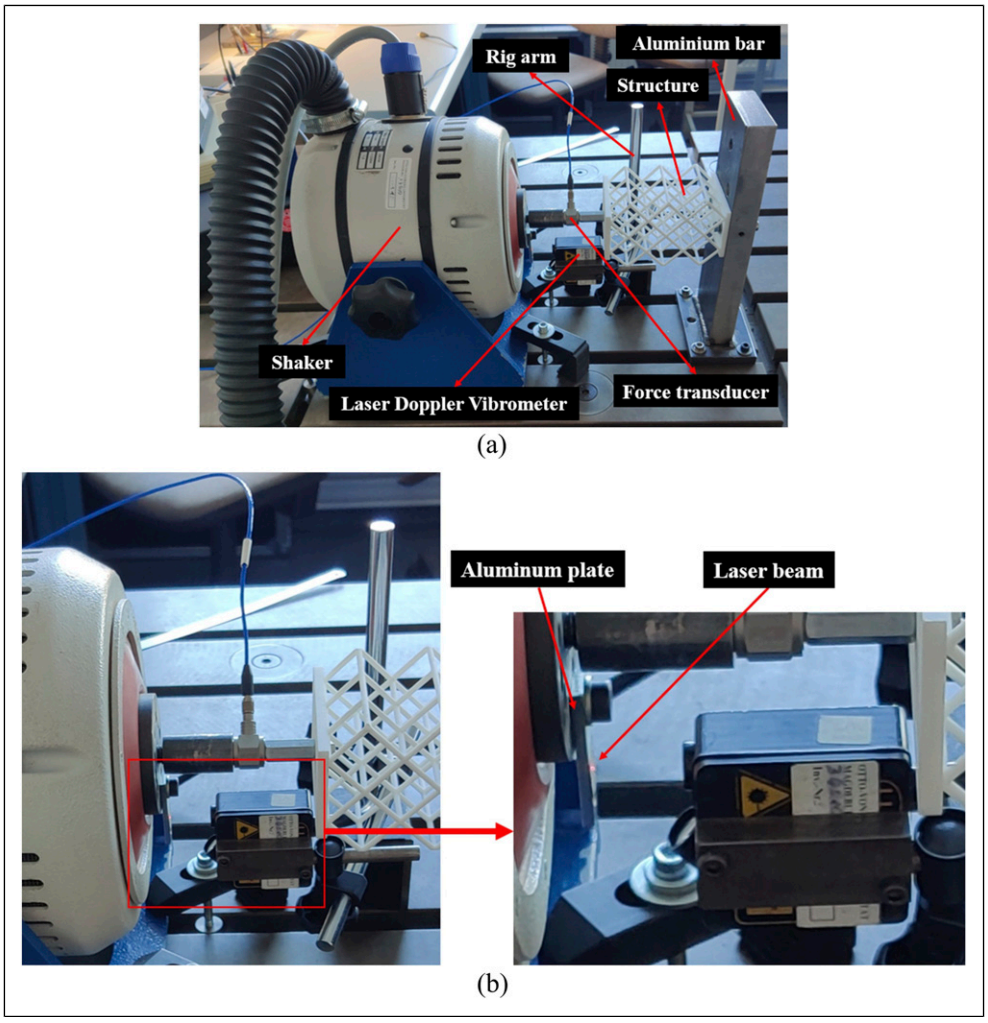

Figure 5. (a) The experimental setup, and (b) the setup of the laser doppler vibrometer for displacement measurement.

$$c = \frac{E_D}{\pi \omega {u_0}^2} \tag{5}$$

where E_D signifies the energy dissipated per cycle of harmonic oscillation, u_0 represents the lattice's displacement amplitude, and ω denotes the excitation frequency. E_D was determined from the measured force–displacement hysteresis loops using a custom MATLAB data-processing routine explained in the subsequent paragraph:

The displacement $u(t)$ and applied force $F(t)$ were recorded during harmonic excitation with a sampling frequency of 100 kHz. To reduce measurement noise while preserving the phase relationship between the signals, both channels were filtered using a fourth-order Butterworth low-pass filter implemented with zero-phase forward–backward filtering (filtfilt). The cutoff frequency f_c was defined as

$$f_c = 3\frac{\omega}{2\pi} + 50 \text{ Hz} \tag{6}$$

Before further analysis, the mean values of displacement and force signals were removed to eliminate sensor offsets. Solely the steady-state portion of the measurement was used for E_D calculation. The processing routine automatically excluded the initial transient response and retained the later portion of the signal containing approximately ten complete excitation cycles. Individual cycles were identified using zero-crossings of the velocity signal, obtained by numerical differentiation of the displacement data.

The energy dissipation for each cycle was computed as the enclosed area of the force–displacement (u, F) hysteresis loop

$$E_D = \oint F \, du \tag{7}$$

which was evaluated numerically using the MATLAB polyarea function applied to the discrete (u, F) data points of each cycle. The final E_D value reported in this work corresponded to the average over multiple steady-state cycles, which reduces the influence of measurement noise and cycle-to-cycle variability. The combination of high sampling frequency, zero-phase filtering, transient removal, and cycle averaging ensured robust estimation of the hysteresis loop area.

The maximum strain energy E_S was calculated as

$$E_S = \frac{1}{2}\widehat{F}u_0 \tag{8}$$

where $\widehat{F}$ is the force magnitude. By using the above equation of maximum strain energy E_S, substituting the Hooke's law $(\widehat{F} = ku_0)$ into Eq. 8, and rearranging the equation, the stiffness k can be obtained as

$$k = 2\frac{E_S}{{u_0}^2} \tag{9}$$

The energy loss factor η crucial for a comprehensive comparison of damping behaviours between regular and irregular lattice structures is defined as follows:

$$\eta = \frac{1}{2\pi}\frac{E_D}{E_S} \tag{10}$$

2.3. Normal modes and frequency response analyses

Generally, the FRA quantifies the steady-state response resulting from the imposition of a sinusoidal load onto a structural system. In addition, normal modes analyses are utilised to investigate a structure's dynamic properties. In the framework of this investigation, the FRA was employed to ascertain the magnitudes and phase shifts of displacements in lattice structures subjected to the experimental loading conditions. The normal modes analyses predicted lattice's eigenfrequencies.

Figure 6 exemplarily shows the numerical model setup of RL2. Each strut of the lattices was modelled using CBEAM

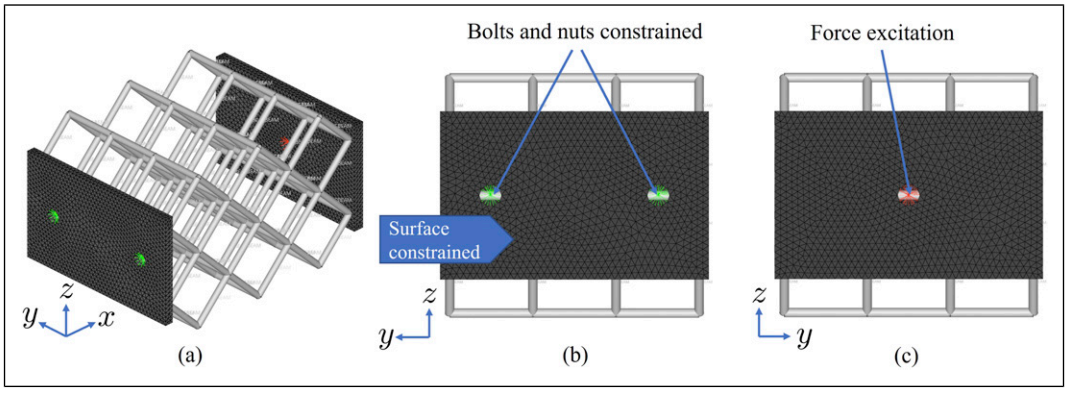

Figure 6. (a) Isometric view, (b) aluminium bar side, and (c) shaker side of the numerical model of RL2. Beam elements are shown in light grey, 3D tetrahedral elements in dark grey, and rigid body elements RBE2 are coloured in green (fixations) and red (force excitation).

Table 4. Mesh sensitivity analysis results for the RL2 lattice model showing the normalised natural frequencies of the first three modes depending on the beam element size.

Beam element size (mm)	12.37	8.25	6.19	4.95	4.12	3.54	3.09	2.75
1st eigenfrequency	0.992	0.996	0.997	0.999	0.999	1.000	1.000	1.000
2nd eigenfrequency	0.993	0.996	0.998	0.998	0.999	1.000	1.000	1.000
3rd eigenfrequency	0.992	0.996	0.997	0.999	0.999	1.000	1.000	1.000

elements. They were connected to the plates using rigid body elements RBE2 elements. Both rectangular plates were meshed with 3D tetrahedral elements (CTETRA). As for the boundary conditions, the two boreholes on the rectangular plate (see Figure 6(b)) were fixed with spider RBE2s in all degrees of freedom to mimic the constraint from the bolts and nuts. In addition, the elements on the surface of the rectangular plate were constrained in the x direction to mimic the friction constraint between the aluminium bar and the lattice. For the condition of the rectangular plate on the shaker side (see Figure 6(c)), a spider RBE3 was created at the bore hole, and a harmonic excitation force in the x direction was applied to the spider element's centre to simulate the force exerted by the shaker.

A mesh sensitivity analysis was conducted to ensure that the numerical results were not significantly influenced by the discretisation of the finite element model. The RL2 lattice configuration was selected as a representative case, and the beam element size used for the lattice struts was gradually reduced from 12.37 mm to 2.75 mm. The solid elements representing the rectangular plates were kept constant with a comparably small element size of 1 mm.

The mesh sensitivity analysis focused on the lattice structure itself, whereas the rectangular plates mainly served as relatively stiff supporting components. Moreover, the solid element size of 1 mm was already comparable to the characteristic geometric scale of the lattice struts, indicating that the plates were sufficiently discretised. In addition, the connection between the beam elements of the lattice and the solid elements of the rectangular plates was implemented using RBEs. Changing the mesh density of the plates would have modified the distribution of coupling nodes and could have altered the stiffness characteristics of the beam-solid connection region in a non-physical manner. Therefore, the mesh refinement study was carried out only for the beam elements of the lattice while maintaining a consistent discretisation of the boundary plates.

The convergence behaviour was evaluated using the first three natural frequencies obtained from modal analysis. To facilitate comparison across different modes, the frequencies were normalised with respect to the finest mesh solution (2.75 mm element size). As shown in Table 4, the normalised frequencies approached unity as the mesh was refined, indicating that the predicted natural frequencies became nearly constant when the beam element size was approximately 3.54 mm or smaller. Based on this observation, a beam element size of 3.09 mm was adopted for the lattice structures in the numerical simulations, which permitted also the representation of gradually changing cross-section diameters along one strut implemented in lattices IL1 and IL4.

To obtain better agreement between the experimental and numerical results, an empirical iterative calibration procedure was adopted. The structural damping coefficient GE defined in the MAT1 material card (isotropic material) was tuned individually for each lattice configuration to reproduce the experimentally observed damping behaviour. In this formulation, the damping matrix contribution $[K_{GE}]$ is introduced as a scaling factor of the stiffness matrix $[K]$, which can be expressed as (HyperWorks, 2021)

$$[K_{GE}] = GE\ [K] \tag{11}$$

To assess the influence of the selected GE, the same harmonic excitation forces used in the experiments were applied in the numerical simulations. The calibrated values of GE for each lattice configuration are summarised in Table 5.

After specifying the boundary conditions and the forces, a normal modes analysis and a direct FRA were performed. For the normal modes analysis, the first eigenfrequency of the lattices was predicted by solving the eigen-solution problem using the Lanczos eigenvalue extraction method available in Altair OptiStruct. Regarding the FRA, the obtained displacement amplitude and phase angle values for each lattice were extracted from the numerical output file for subsequent data using equations (5)–(10). The resulting damping coefficient, stiffness, and loss factor were subsequently compared with the experimental findings. The

Table 5. *GE* value used for the MAT1 card for each lattice structure.

Lattice	*GE*
RL1	0.17
RL2	0.16
IL1	0.16
IL2	0.16
IL3	0.18
IL4	0.17

percentage of deviation Δr was calculated using the following equation

$$\Delta r = \frac{r_n - r_e}{r_e} \cdot 100 \tag{12}$$

where r_n and r_e are the numerical and experimental result, respectively.

3. Results

In this section, the results of the experimental and numerical investigation of both regular and irregular lattice structures are presented.

3.1. Experimental results

The experiments were successfully conducted for all structures. Figure 7(a) shows exemplarily the measured force plotted against time for RL1 at 5 Hz, which accurately represents the input conditions of the experiment, that is, a sinusoidal force at a frequency of 5 Hz. The measured displacement against time for RL1 at 5 Hz (Figure 7(b)) exhibited sinusoidal behaviour, reflecting the system's dynamic response. Notably, the displacement amplitude responded with a phase shift relative to the applied force. This phase shift is indicative of the system's damping characteristics and is a critical parameter for further analysis. The hysteresis loop for RL1 at an excitation frequency of 5 Hz is visible in Figure 7(c). The results for the remaining studied excitation frequencies as well as for the other studied lattice structures, and the calculated values for E_D and E_S are attached in the supplemental materials.

Figure 8 presents the damping coefficient c, the stiffness k, and the loss factor η for each lattice at the studied excitation frequencies, calculated based on the experimental results and equations (5)–(10). Generally, the damping coefficient decreased gradually, approaching zero as the excitation frequency increased. All lattice structures exhibited the highest damping coefficient when excited at 5 Hz (between 172.78 Ns/m for the RL1 and 1725.38 Ns/m for the IL4). Regarding the stiffness, IL2, IL3, and IL4 showed values exceeding 200,000 N/m, markedly higher than those of RL1, RL2, and IL1, all of which remained below 50,000 N/m across all investigated frequencies. Overall, when comparing irregular and regular lattices, the former demonstrated superior performance in terms of both damping coefficient and stiffness values across all frequencies compared to the latter.

In the case of the loss factor, the values consistently dropped from 5 Hz to 20 Hz across all lattice types. However, when extending the analysis to the higher bandwidth, greater fluctuations in the loss factor became apparent including significantly different values at specific frequencies, especially for the irregular lattices. In some instances, the loss factor experienced remarkable drops or spikes (e.g. for IL2, $\eta > 0.2$ at 35 Hz, but $\eta < 0.07$ at 30 Hz and 40 Hz, or for IL4, $\eta < 0.04$ at 40 Hz, but $\eta > 0.06$ at 35 Hz and 45 Hz).

Regarding lattice IL2, the pronounced local peak of the loss factor at around 35 Hz excitation frequency was likely caused by a frequency-dependent redistribution of deformation within the irregular lattice, which led to a temporary increase in dissipated energy relative to the maximum strain energy. Since the loss factor is defined as stated in equation (10), even a localised non-proportional change in these two quantities can produce a sharp peak. The fact that a similar tendency has also been observed in the numerical results suggests that this feature is related to the structural response of IL2 rather than to measurement noise alone.

Generally, in most of the studied frequencies, the irregular lattice showed higher loss factors than the regular lattices.

3.2. Numerical results

This subsection presents a comparison between experimental and numerical results to evaluate the accuracy of the numerical models in representing the physical reality of the studied lattice structures.

Figures 9 and 10 exemplarily show the damping constant, loss factor, and stiffness based on the measurements and the

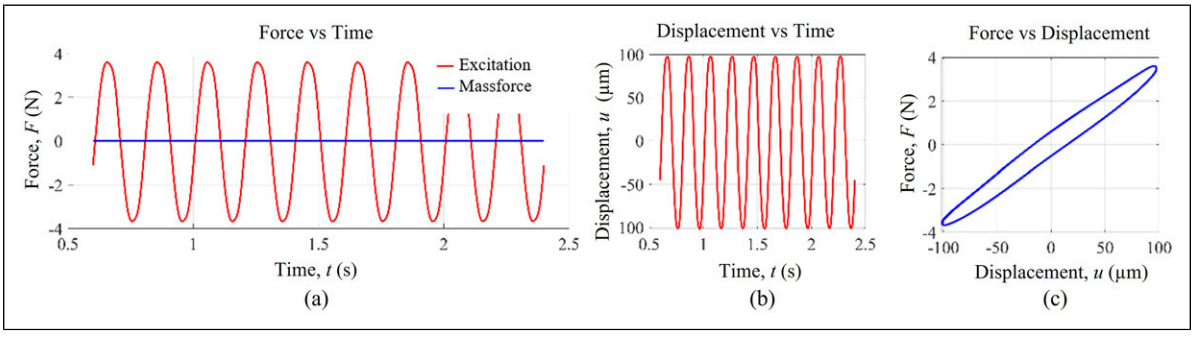

Figure 7. Experimental results of RL1 at 5 Hz excitation force including (a) the measured force plotted against time, (b) the measured displacement against time, and (c) the hysteresis loop.

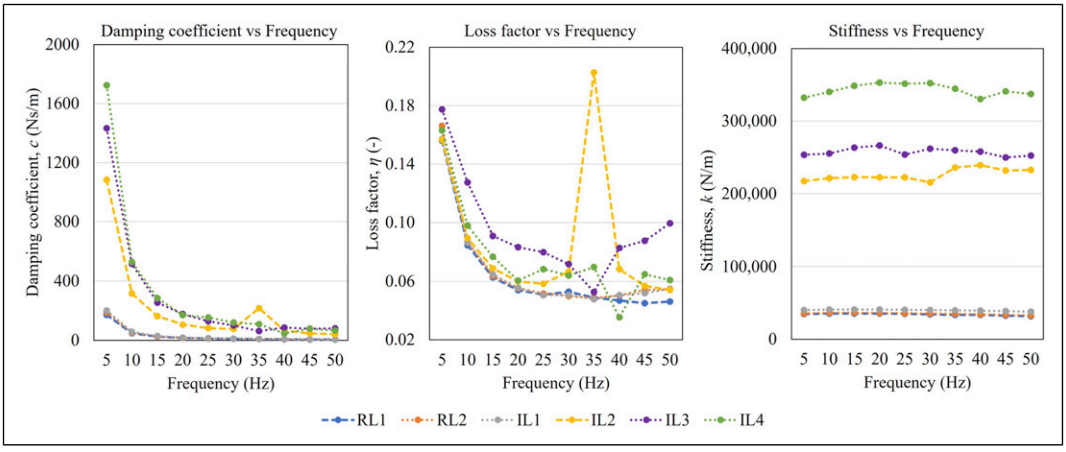

Figure 8. Damping coefficient *c*, loss factor η, and stiffness *k* versus frequency of each lattice at every excitation frequency obtained from experiments.

numerical model for RL2 and IL2, respectively. The displayed curves align very well. Generally, for all investigated lattice structures, the average deviation between experimental and numerical values for all three parameters remained less than 3% across all studied excitation frequencies.

Regarding the first eigenfrequency of each lattice (Table 6), the studied regular lattices, on average, showed a lower first eigenfrequency than the irregular lattices. However, the first eigenfrequency of IL1 is comparably low, that is, lower than that of RL2. Table 6 also compares the mass of the numerical models to that of the manufactured models. The mass deviations were between 2.2% and 8.4%.

4. Discussion

This section discusses obtained numerical and experimental results.

4.1. Numerical results in comparison to experimental results

The numerical and experimental results showed high congruence in curve paths, exemplarily presented for RL2 and IL2 (c.f., Figures 9 and 10) indicating a high degree of accuracy in the numerical models. Despite the small percentage of differences observed in the structural mass, the obtained results were well correlated.

The outcomes of this comparison provide evidence that the FE models created can reliably represent the dynamic behaviour of the studied physical structures across the interested range of excitation frequencies. This suggests that these models can confidently be utilised in any subsequent analyses similar to the conducted analyses, ensuring the reliability and precision of numerical predictions.

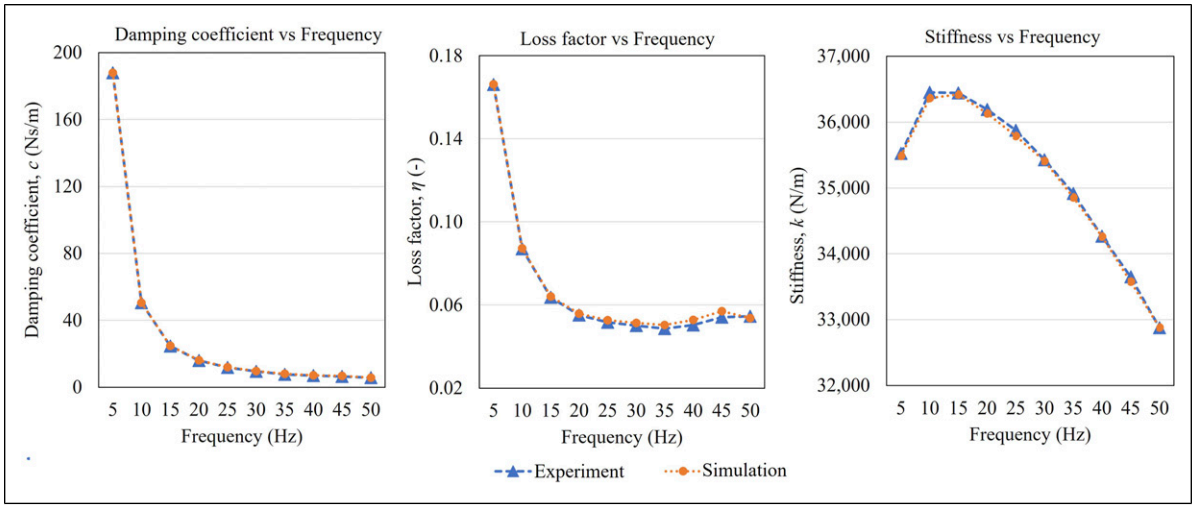

Figure 9. Damping coefficient *c*, loss factor η, and stiffness *k* versus frequency of RL2 at every excitation frequency based on experiments (blue data) and simulation (orange data).

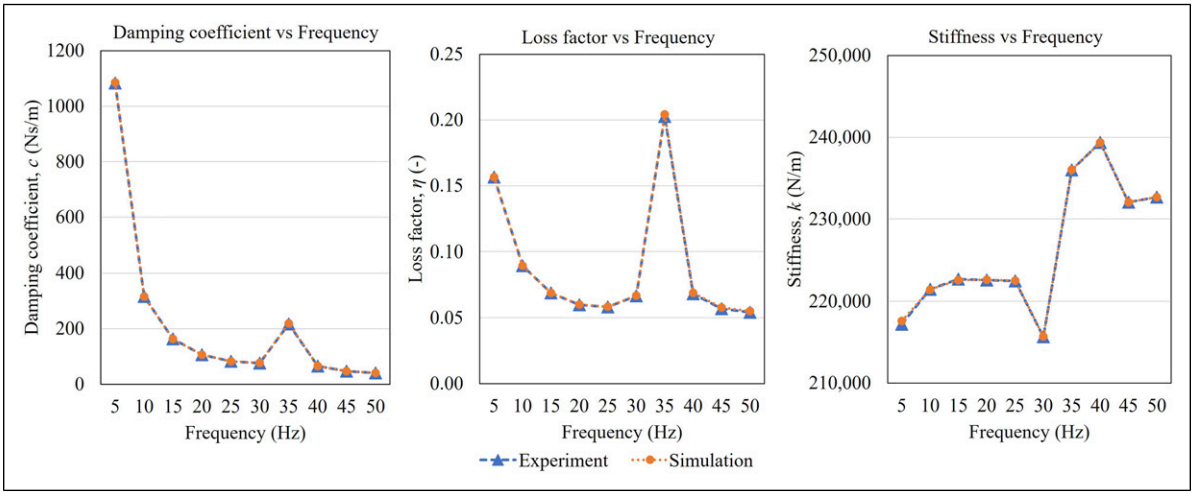

Figure 10. Damping coefficient c, loss factor η, and stiffness k versus frequency of IL2 at every excitation frequency based on experiments (blue data) and simulation (orange data).

4.2. Lattice design and manufacturing

The successful creation of the lattice structures varying in their degrees of structural complexity sets the stage for the subsequent exploration of the lattice damping behaviour. Through the control of design variables and modelling techniques, this study offers valuable insights into the impact of irregularities in lattice structures on the damping characteristics.

Six different lattices were successfully designed and manufactured in this study. The structures encompassed both regular and irregular lattice structures, each meticulously built within the defined design space. Regular lattices adhered to predictable patterns, while irregular ones introduced complexity through varying cross-section diameters and irregularly oriented strut layouts.

All studied lattices coincided in their mass. Maintaining consistent mass across all lattice structures ensured that observed damping differences stemmed primarily from geometric variations rather than mass discrepancies. Additionally, comparing the masses of the numerical models to those of the manufactured structures showed differences of less than 8%, indicating a successful manufacturing process. The small deviation in mass between the FE models and the manufactured lattices can be attributed to the modelling approach employed, as discussed in Andresen et al. (2020a). The utilisation of CBEAM elements to construct each of the struts resulted in a marginal increase in mass, as each strut was represented as a full beam, thereby attributing the entire mass of a single beam to each strut, regardless of their merging at common intersection points. Consequently, the overall mass calculated within the FE model slightly exceeded that of the manufactured lattices.

4.3. Effect of lattice design parameters on dynamic properties

This section discusses the impact of structural parameters employed in the studied lattices on the loss factor, the damping coefficient, the stiffness, and the eigenfrequencies.

4.3.1. Unit cell size in regular lattices. The investigated regular lattices were both composed of simple cubic unit cells permitting a comparison in terms of the unit cell size. The loss factor of RL2 (large unit cell) maintained a slightly higher value than that of RL1 (small unit cell) at most frequencies (Figure 11). Similarly, the damping coefficient of RL2 slightly surpassed that of RL1 across almost the entire frequency spectrum. These findings may indicate that for the studied unit cell type, a larger unit cell size exhibits a greater propensity for dissipating energy, suggesting its potential superiority in vibration absorption. Moreover, RL2 also shows a higher stiffness value than RL1 at all frequencies, which suggested that it may not be as flexible as RL1, but still manages to offer a slightly enhanced damping effect, particularly at higher frequencies. This might be attributed to an increase in the overall area moment of inertia as the strut diameter size rose (Azmi et al., 2020), resulting in enhanced stiffness of the RL2 structure. At the same time, similar to the stiffness, the eigenfrequency is also higher than that of RL1.

In similar experiments conducted on regular lattices composed of body-centred cubic unit cells varying in unit cell sizes (Monkova et al., 2021), the results showed decreases in damping behaviour with increasing stiffness and eigenfrequencies, which were not observed here. In contrast, the damping behaviour of the studied regular lattices tends to slightly increase with increasing unit cell size, stiffness, and eigenfrequencies. A similar trend was also observed by Liu and Faisal (2022). However, Scalzo et al. (2021) did not

Table 6. Mass comparison between the numerical and manufactured models.

Model	Eigenfrequency (Hz)	Numerical mass (g)	Manufactured mass (g)	Deviation (%)
RL1	44.09	58.27	55.24	5.48
RL2	52.07	58.95	55.29	6.62
IL1	46.13	58.08	54.02	7.51
IL2	96.99	58.38	55.14	5.87
IL3	129.13	58.51	53.98	8.39
IL4	125.47	58.97	57.68	2.23

discover a clear correlation between unit cell size, stiffness, eigenfrequency, and damping behaviour. Therefore, in future studies, a higher number of regular lattices including varying unit cell sizes and different unit cell designs should be studied in order to meticulously assess the effect of unit cell styles on the dynamic characteristics.

4.3.2. Gradient regular and irregular lattice structures. The application of strut cross-section gradients has been implemented in a regular and an irregular lattice structure, which have also been investigated with a constant cross-section diameter, permitting a first step into studying the impact of cross-section diameter gradients on damping properties and stiffness. Cross-section diameter gradings are irregular cross-section distributions within a structure. Here, it was focussed on variations in diameters of circular strut cross-sections.

Figure 12 offers insights into how the strut cross-section gradients influenced the damping properties and stiffness of lattice IL1 compared to RL2, both lattices having the same regular lattice strut layout. Although IL1 exhibited a distinct mass distribution due to the gradually increasing cross-section diameter towards the structure's centre, the damping properties at all analysed frequencies were similar to those from RL2. Thus, the defined cross-section gradient applied to IL1 may not exert a substantial influence on its damping properties. However, the gradient definition resulted in an overall stiffer structure compared to the uniform strut size of RL2, which is in line with the outcome presented by Sienkiewicz et al. (2020).

With regard to strut cross-section gradients employed in irregular lattices, IL4 (gradually changing cross-section) shows a higher stiffness compared to IL3 (uniform cross-section) (Figure 13), as also obtained for the regular lattices. However, in contrast to the preceding comparison of regular lattices, the assessment of the cross-section diameter gradient also revealed a notable influence on both the loss factor and damping coefficient. IL4 notably surpassed IL3 in terms of the damping coefficient for most of the studied frequencies. In addition, more pronounced fluctuations in their loss factors across the entire frequency range have been detected. This discovery indicates the significant potential of cross-section gradients to profoundly affect damping characteristics within lattice structures.

The concept of cross-section strut gradients influencing damping properties is neither limited to a specific lattice layout nor to certain gradient definitions. It became apparent

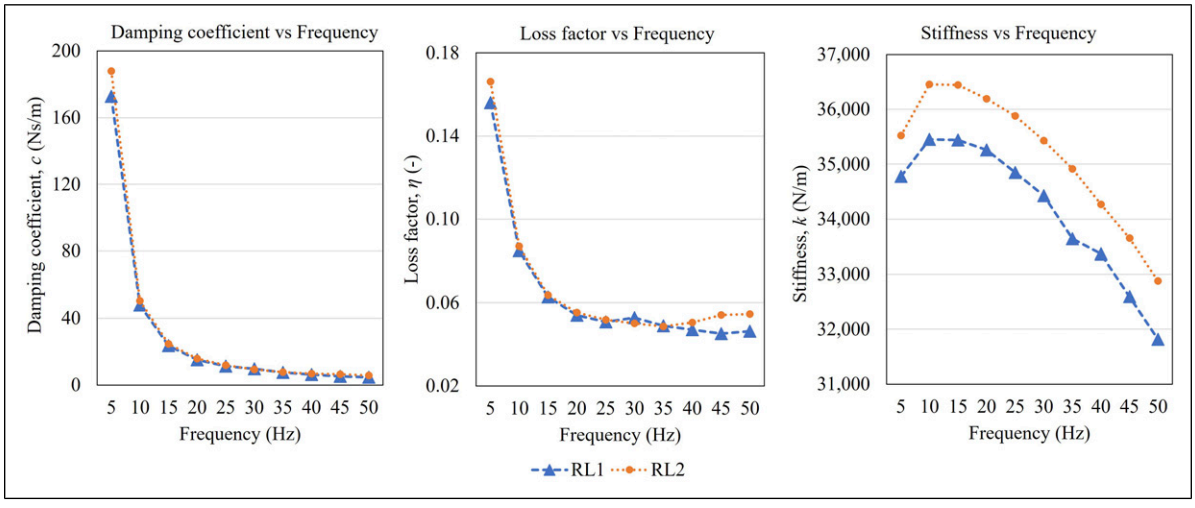

Figure 11. Comparison graphs of damping coefficient c, loss factor η, and stiffness k versus frequency for RL1 and RL2 obtained from experiments.

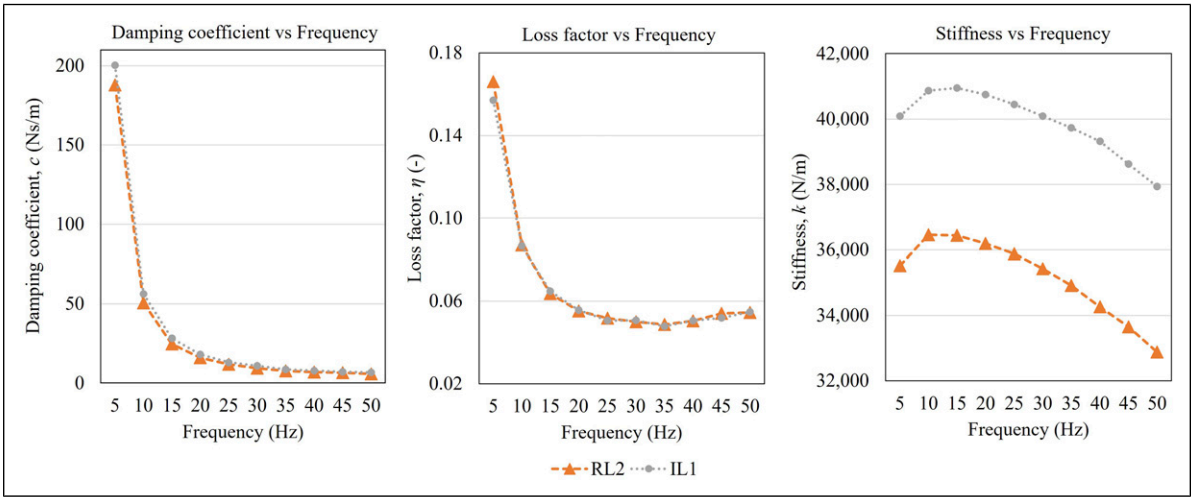

Figure 12. Comparison graphs of damping coefficient c, loss factor η, and stiffness k versus frequency for RL2 and IL1 obtained from experiments.

that precise definitions of gradients are essential, as evidenced by its negligible impact on the damping properties of the regular lattice strut layout. Beyond the specific gradient applied to IL1, for example, further studies could delve into alternative grading definitions to assess their impact on damping properties. However, although the here obtained results for the regular lattices did not show improved damping properties of the graded lattice structure, published studies demonstrated that varying strut cross-section diameters in regular lattices can strongly affect the damping behaviour (Scalzo et al., 2021). It may be noted that Scalzo et al. (2021) investigated lattices with different constant cross-section diameters.

Regarding the definition of cross-section gradients, a proper definition is expected to significantly enhance the damping properties. Therefore, in future studies, different cross-section gradient definitions should be investigated to significantly enhance the damping properties. One such variation could involve an increase in strut size from left to right or vice versa, akin to the deformation observed in a crushed lattice structure as shown by Okubo et al. (2023). By mimicking such deformation-induced gradients, the impact of asymmetrical cross-section distributions on damping behaviour can be evaluated. Additionally, other gradient schemes such as exponential or logarithmic variations in cross-sectional area could also be explored to capture more complex structural responses. These alternative gradient definitions can also be applied to irregular lattices to further improve the damping properties. Aside from the here investigated circular cross-sections, different

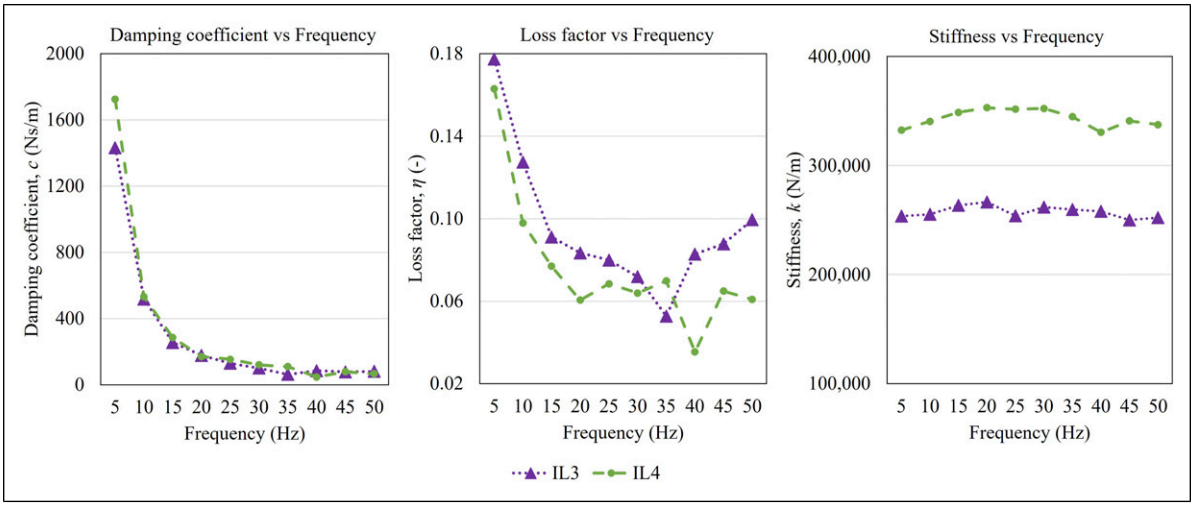

Figure 13. Comparison graphs of damping coefficient c, loss factor η, and stiffness k versus frequency for IL3 and IL4 obtained from experiments.

cross-section shapes could also be studied and varied within one structure based on specified gradients.

Finally, comparing the obtained eigenfrequencies for the lattices with cross-section gradients to those without gradients, in both the regular and irregular lattices, the defined cross-section grading resulted in an eigenfrequency drop. In a similar study by Andresen et al. (2020a), cross-section gradients in lattices led to significant eigenfrequency increases. However, Andresen et al. (2020a) performed optimisations to obtain optimum cross-section diameters, while in the present study, a random definition of cross-section gradients was applied. This underscores once again the conclusion that a detailed study on the impact of different cross-section gradient definitions on the vibration characteristics is needed, because proper specifications of cross-section gradients have a high potential in improving not only the damping properties but also the eigenfrequencies.

4.3.3. Irregular lattices in comparison to regular lattices. The findings presented in this study revealed a noteworthy trend in the performance of the studied irregular lattices in comparison to the studied regular lattices. The investigated irregular lattices exhibited a more intricate and frequency-sensitive response. While the regular lattices showed a smoother, monotonous decline in the loss factor with increasing frequency, irregular lattices introduced complexity, manifesting as fluctuations and sharp variations at specific frequencies. The results also indicate that the lattices exhibiting a higher damping and stiffness generally correspond to larger values of the I_{irr} but still in a frequency-dependent manner. At the same time, the comparison between RL2 and IL1 suggests that the specific type of irregularity also plays an important role, since introducing solely a cross-section gradient seems to affect the damping enhancement less strongly than irregular strut layouts. However, further detailed studies are needed to underline this hypothesis.

Comparing the optimum regular lattice RL2 to the optimum irregular lattice IL3 (Figure 14), the latter had a significantly higher value in all studied characteristics than RL2. By their very nature, irregular lattices introduce a level of complexity and variability in their geometric arrangements. This complexity might result in a broader range of vibrational modes and energy dissipation mechanisms within the structure as discussed in Zheng et al. (2005) in Alkhatib et al. (2023). As a consequence, irregular lattices display enhanced damping and stiffness properties, making them particularly effective in dissipating energy and maintaining structural stability, even when subjected to varying frequencies of excitation. In addition, regular and irregular lattices probably differ in their way of how the forces are distributed across the structure. Lattice structures with highly regular unit cells like RL2 have symmetrical and uniform geometries. These regular geometries of unit cells can result in evenly distributed forces. While this can provide structural stability, it might also limit the structure's ability to dissipate energy as efficiently, leading to a lower loss factor and less effective damping. The random point distribution in IL3, on the other hand, may introduce variations in stress distribution. These variations can provide additional opportunities for energy dissipation, potentially resulting in a higher loss factor and better damping characteristics. Furthermore, a significant difference can be seen where a random point distribution in IL3 leads to a high-stiffness value compared to a repeating unit cell pattern (Andresen et al., 2020a).

An important observation across both irregular and regular lattices is the consistent decrease in the damping coefficient and loss factor as the excitation frequency increased. This behaviour is in line with the general trend in structural dynamics, where higher frequencies tend to yield decreased energy dissipation and damping capability (Benyoucef et al., 2017; De Lima et al., 2014; Verbaan et al., 2017). Such a finding underscores the critical role of frequency in influencing the dynamic response of lattice structures and provides valuable insights for applications where precise control of damping and stiffness is required.

Furthermore, the studied irregular lattices exhibited a superior damping coefficient and stiffness characteristics consistently, regardless of the frequency of excitation. The reason for this observed outcome can be inferred based on the characteristics that the irregular lattice structures possessed.

In general, the analysis of irregular strut layouts presents challenges in formulating generalised statements about their behaviour, primarily due to the limited number of studied lattices and significant structural disparities among them. There is 'almost no limit' in variety of irregular lattices. Nevertheless, the obtained results suggest a tendency for irregular lattices to exhibit superior performance compared to their regular counterparts. Moreover, the notable advantage of irregular lattices lies in the flexibility afforded by the positioning of struts wherever they contribute positively to the studied parameters. This inherent flexibility grants designers nearly limitless freedom in crafting irregular lattice layouts. While this presents both challenges and opportunities, as determining the optimal strut layout and recognizing when the best configuration is achieved remain formidable tasks, it also signifies a remarkable opportunity for innovation and optimisation in lattice structure design. To deepen the understanding of this aspect, future studies should encompass a larger and more diverse selection of regular and irregular lattice configurations. Moreover, the structural parameters should be systematically varied or adapted to elucidate the precise impact of structural characteristics such as the number of joints, distance between neighbouring joints, angle between struts, and the connectivity of joints on the parameters under investigation. This iterative approach will facilitate a more comprehensive

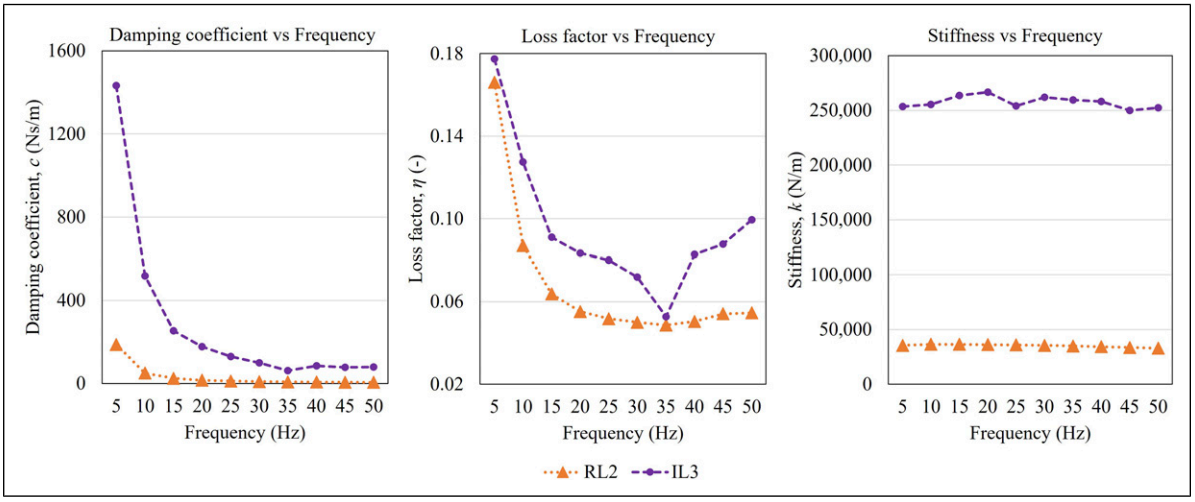

Figure 14. Comparison graphs of damping coefficient c, loss factor η, and stiffness k versus frequency for RL2 and IL3 obtained from experiments.

exploration of the relationships between lattice morphology and performance metrics.

In conclusion, the findings of this study highlight the potential advantages of irregular lattice designs in terms of damping and stiffness performance. These results underscore the importance of considering structural irregularities as a design parameter in lattice engineering, offering opportunities for optimising performance across a range of engineering applications. Future research endeavours should aim to delve deeper into the underlying mechanisms and design principles governing the behaviour of irregular lattice structures, with the ultimate goal of advancing the state-of-the-art in lattice design and optimisation.

In terms of the conducted numerical analyses, the following remarks may be noted. Despite the present positive outcomes from the numerical work, it is essential to acknowledge the inherent limitations of simulation models. While simulations can provide valuable insights into the behaviour of lattice structures, they rely on assumptions and simplifications that may not fully capture all real-world complexities. Additionally, the accuracy of simulation results is contingent upon the fidelity of the computational model and the validity of the underlying assumptions.

Simulation models offer a promising avenue for studying additional lattice configurations; however, their suitability depends on factors such as the fidelity of the model, the complexity of the phenomena under investigation, and the availability of experimental validation. By judiciously leveraging both simulation and experimental approaches, researchers can synergistically enhance their understanding of lattice behaviour and advance the state-of-the-art in lattice design and optimisation.

Regarding the calibration of the *GE* values for each lattice to improve the numerical representation of the experiments, it should be noted that this calibration improved the agreement between numerical and experimental results, but reduced the predictive capability of the model, since the damping parameter was not determined solely from material or geometric properties. The present approach therefore aims to reproduce the experimentally observed dynamic response within the investigated frequency range with an adequate engineering judgement. Future developments could focus on introducing a unified damping parameter or a physically motivated damping formulation that accounts for the dominant dissipation mechanisms in the lattice structures, which would enhance the general applicability of the modelling framework. While the use of a unified damping parameter could improve the consistency of the numerical model, a physically motivated damping formulation that accounts for the dominant energy dissipation mechanisms would further enhance its predictive capability and general applicability.

5. Conclusion

The present study shows that the use of bio-inspired irregular lattice strut layout can significantly increase the stiffness, the eigenfrequencies, and the damping properties (i.e. damping coefficient and loss factor) compared to regular lattices based on unit cells. Thereby, the obtained experimental data indicate that the damping and stiffness performance of the investigated lattices generally increase with the proposed geometric irregularity index I_{irr}, also suggesting a high impact of the specific type of irregularity. While only a limited number of lattice structures have been investigated, the results already demonstrate the high potential of these complex lightweight structures to strongly manipulate vibration properties. This innovation paves the way for the creation of lightweight structures inspired by

biological structures that excel in managing vibrations, offering versatile solutions across a spectrum of engineering applications.

Acknowledgements

The authors acknowledge the input and support from Dr.-Ing. Christian Daniel and Prof. Dr.-Ing. Elmar Woschke from the Institute of Mechanics, Otto von Guericke University Magdeburg, Germany, during the experimental work. In addition, we acknowledge support by the Open Access publication fund of Alfred-Wegener-Institut Helmholtz-Zentrum für Polar-und Meeresforschung.

ORCID iDs

Ahmad Burhani Ahmad Basri https://orcid.org/0000-0002-4877-0341

Simone Andresen https://orcid.org/0000-0002-3873-7089

Funding

The authors disclosed receipt of the following financial support for the research, authorship, and/or publication of this article: This research was funded by the Innovation Fund from the Alfred Wegener Institute, Helmholtz Centre for Polar and Marine Research (AWI), and by the Deutsches Elektronen-Synchrotron (DESY), a research facility of the Helmholtz Association.

Declaration of conflicting interests

The authors declared no potential conflicts of interest with respect to the research, authorship, and publication of this article.

Supplemental material

Supplemental material for this article is available online.

References

Adhikari M (2023) *Diatom Inspired Bridge Design*. Master's Thesis. Åbo Akademi University. https://www.doria.fi/bitstream/handle/10024/187636/adhikari_mukunda.pdf?sequence=3

Alkhatib SE, Karrech A and Sercombe TB (2023) Isotropic energy absorption of topology optimized lattice structure. *Thin-Walled Structures* 182: 110220. https://doi.org/10.1016/j.tws.2022.110220

Andresen S (2021) Impact of bio-inspired structural irregularities on plate eigenfrequencies. In: Sapountzakis EJ, Banerjee M, Biswas P, et al. (eds) Proceedings of the 14th international conference on vibration problems. Springer Nature Singapore, pp. 1117–1125. https://doi.org/10.1007/978-981-15-8049-9_71

Andresen S and Ahmad Basri AB (2024) Diatom-inspired structural adaptation according to mode shapes: a study on 3d structures and software tools. *Biomimetics* 9(4): 241. https://doi.org/10.3390/biomimetics9040241

Andresen S, Bäger A and Hamm C (2020a) Eigenfrequency maximisation by using irregular lattice structures. *Journal of Sound and Vibration* 465: 115027. https://doi.org/10.1016/j.jsv.2019.115027

Andresen S, Lottes LM, Linnemann SK, et al. (2020b) Shape adaptation of beams (1d) and plates (2d) to maximise eigenfrequencies. *Advances in Mechanical Engineering* 12: 1687814020971903. https://doi.org/10.1177/1687814020971903

Andresen S, Meyners N, Thoden D, et al. (2023) Biologically inspired girder structure for the synchrotron radiation facility petra iv. *Journal of Bionic Engineering* 20: 1996–2017. https://doi.org/10.1007/s42235-023-00373-7

Andresen S, Linnemann SK, Ahmad Basri AB, et al. (2024) Natural frequencies of diatom shells: alteration of eigenfrequencies using structural patterns inspired by diatoms. *Biomimetics* 9(2): 85. https://doi.org/10.3390/biomimetics9020085

Ashby MF and Gibson LJ (1997) *Cellular Solids: Structure and Properties*. Press Syndicate of the University of Cambridge.

Azmi M, Ismail R and Hasan R (2020) Investigation on the static and dynamic behavior of bcc lattice structure with quatrefoil node manufactured using fused deposition modelling additive manufacturing. In: *IOP Conference Series: Materials Science and Engineering*. IOP Publishing, Vol. 788, p. 012008. https://doi.org/10.1088/1757-899X/788/1/012008

Azmi MS, Ismail R and Putra A (2022) Correlation of design parameters of lattice structure for highly tunable passive vibration isolator. *Journal of Vibration and Control* 29(7-8): 1777–1790. https://doi.org/10.1177/10775463211070069

Baader J and Fontana M (2017) Active vibration control of lightweight floor systems. *Procedia Engineering* 199: 2772–2777. https://doi.org/10.1016/j.proeng.2017.09.529

Bachir S (2024) Diatom-inspired computational design of radial framework structures: the case of asterolampra. In: Proceedings of IASS Annual Symposia, Volume 2024. International Association for Shell and Spatial Structures (IASS), pp. 1–9. https://www.ingentaconnect.com/contentone/iass/piass/2024/00002024/00000012/art00017

Bai L, Yao H, Han C, et al. (2025) Recent advances in nonlinear vibration metamaterials. *Mechanical Systems and Signal Processing* 236: 113046. https://doi.org/10.1016/j.ymssp.2025.113046

Benyoucef A, Leblouba M and Zerzour A (2017) Stiffness and energy dissipation of oval leaf spring mounts under unidirectional line loading. *Mechanics & Industry* 18(4): 414. https://doi.org/10.1051/meca/2017012

Breish F, Hamm C and Kienzler R (2023) Diatom-inspired stiffness optimization for plates and cellular solids. *Bioinspiration & Biomimetics* 18(3): 036004. https://doi.org/10.1088/1748-3190/acc373

Catchpole-Smith S, Sélo RR, Davis A, et al. (2019) Thermal conductivity of tpms lattice structures manufactured via laser powder bed fusion. *Additive Manufacturing* 30: 100846. https://doi.org/10.1016/j.addma.2019.100846

Chen S, Wang Y, Wu Q, et al. (2025) Autonomous vibration control of beams utilizing intelligent excitation adaptability.

International Journal of Mechanical Sciences 293: 110194. https://doi.org/10.1016/j.ijmecsci.2025.110194

Cheng L, Liang X, Belski E, et al. (2018) Natural frequency optimization of variable-density additive manufactured lattice structure: theory and experimental validation. *Journal of Manufacturing Science and Engineering* 140(10): 105002. https://doi.org/10.1115/1.4040622

De Lima A, Guaraldo-Neto B, Sales T, et al. (2014) A time-domain modeling of systems containing viscoelastic materials and shape memory alloys as applied to the problem of vibration attenuation. *Engineering Structures* 68: 85–95. https://doi.org/10.1016/j.engstruct.2014.02.035

Do G, Geißelbrecht M, Schwieger W, et al. (2020) Additive manufacturing of interpenetrating periodic open cellular structures (interpocs) with in operando adjustable flow characteristics. *Chemical Engineering and Processing: Process Intensification* 148: 107786. https://doi.org/10.1016/j.cep.2019.107786

D'Mello Y, Bernal S, Petrescu D, et al. (2022) Solar energy harvesting mechanisms of the frustules of Nitzschia filiformis diatoms. *Optical Materials Express* 12(12): 4665–4681. https://doi.org/10.1364/OME.473109

Evans AG, He M, Deshpande VS, et al. (2010) Concepts for enhanced energy absorption using hollow micro-lattices. *International Journal of Impact Engineering* 37(9): 947–959. https://doi.org/10.1016/j.ijimpeng.2010.03.007

Feng Y, Wang Y, Wu Q, et al. (2026) Stiffness-inverting low-profile metamaterial pair for large-stroke quasi-zero-stiffness vibration isolation. *International Journal of Mechanical Sciences* 312: 111225. https://doi.org/10.1016/j.ijmecsci.2026.111225

Gibson L (1985) The mechanical behaviour of cancellous bone. *Journal of Biomechanics* 18(5): 317–328. https://doi.org/10.1016/0021-9290(85)90287-8

Gibson LJ (1989) Modelling the mechanical behavior of cellular materials. *Materials Science and Engineering: A* 110: 1–36. https://doi.org/10.1016/0921-5093(89)90154-8

Hamm CE (2005) The evolution of advanced mechanical defenses and potential technological applications of diatom shells. *Journal of Nanoscience and Nanotechnology* 5(1): 108–119. https://doi.org/10.1166/jnn.2005.023

Hamm CE, Merkel R, Springer O, et al. (2003) Architecture and material properties of diatom shells provide effective mechanical protection. *Nature* 421(6925): 841–843. https://doi.org/10.1038/nature01416

Hamm C, Siegel D, Niebuhr N, et al. (2015) Offshore foundation based on the Elise method. In: *Evolution of Lightweight Structures: Analyses and Technical Applications*. Springer, pp. 195–206. https://doi.org/10.1007/978-94-017-9398-8_12

Han Y and Lu WF (2018) A novel design method for nonuniform lattice structures based on topology optimization. *Journal of Mechanical Design* 140(9): 091403. https://doi.org/10.1115/1.4040546

Heinrichs A, Siegel D, Frank P, et al. (2017) Bionische entwicklung einer additiv gefertigten a-säulen-verstärkung. In: *Karosseriebautage Hamburg 2017: 15. ATZ-Fachtagung*. Springer, pp. 43–56. https://doi.org/10.1007/978-3-658-18107-9_4

HyperWorks A (2021) Altair Optistruct 2021 - User Guide. Available at: https://2021.help.altair.com/2021/hwsolvers/os/topics/solvers/os/user_guide_os_c.htm

Jiangwei L, Kai G, Jie S, et al. (2021) Compressive behavior and vibration-damping properties of porous ti-6al-4v alloy manufactured by laser powder bed fusion. *Journal of Manufacturing Processes* 66: 1–10. https://doi.org/10.1016/j.jmapro.2021.03.060

Koehl M and Strickier JR (1981) Copepod feeding currents: food capture at low Reynolds number 1. *Limnology & Oceanography* 26(6): 1062–1073. https://doi.org/10.4319/lo.1981.26.6.1062

Li M, Wu J, Lin D, et al. (2022) A diatom-based biohybrid microrobot with a high drug-loading capacity and ph-sensitive drug release for target therapy. *Acta Biomaterialia* 154: 443–453. https://doi.org/10.1016/j.actbio.2022.10.019

Li L, Wu J, Yang F, et al. (2025) Mechanisms of low-frequency bandgap formation and energy absorption of three-dimensional nested hybrid lattice structures. *Composites Part B: Engineering* 291: 112045. https://doi.org/10.1016/j.compositesb.2024.112045

Lin C, Wen G, Yin H, et al. (2022) Revealing the sound insulation capacities of tpms sandwich panels. *Journal of Sound and Vibration* 540: 117303. https://doi.org/10.1016/j.jsv.2022.117303

Liu B and Faisal TR (2022) Computational design and fabrication of a bending-active structure using fiberglass: a bioinspired pavilion mimicking marine microorganism radiolaria. *Journal of Bionic Engineering* 19(2): 471–482. https://doi.org/10.1007/s42235-021-00150-4

Ljunggren F and Ågren A (2002) Development of a new damper to reduce resonant vibrations in lightweight steel joist floors. *Applied Acoustics* 63(11): 1267–1280. https://doi.org/10.1016/S0003-682X(02)00025-7

Lu Z, Zhang Q, Fan Q, et al. (2023) Studies on dissipative characteristics and equivalent model of particle damper in railway application. *Journal of Sound and Vibration* 560: 117788. https://doi.org/10.1016/j.jsv.2023.117788

Maier M, Siegel D, Thoben KD, et al. (2013) Transfer of natural micro structures to bionic lightweight design proposals. *Journal of Bionic Engineering* 10(4): 469–478. https://doi.org/10.1016/S1672-6529(13)60241-3

Maskery I, Aboulkhair NT, Aremu A, et al. (2017) Compressive failure modes and energy absorption in additively manufactured double gyroid lattices. *Additive Manufacturing* 16: 24–29. https://doi.org/10.1016/j.addma.2017.04.003

Monkova K, Vasina M, Zaludek M, et al. (2021) Mechanical vibration damping and compression properties of a lattice structure. *Materials* 14(6): 1502. https://doi.org/10.3390/ma14061502

Okubo S, Yamauchi Y and Kitazono K (2023) Effects of random and controlled irregularity in strut lattice structure of pa12 on compression anisotropy. *Additive Manufacturing* 63: 103385. https://doi.org/10.1016/j.addma.2022.103385

Ozdemir Z, Hernandez-Nava E, Tyas A, et al. (2016) Energy absorption in lattice structures in dynamics: experiments. *International Journal of Impact Engineering* 89: 49–61. https://doi.org/10.1016/j.ijimpeng.2015.10.007

Rao SS (2011) *Mechanical Vibrations*. 5th edition. Pearson Ed Asia.

Round FE, Crawford RM and Mann DG (1990) *Diatoms: Biology and Morphology of the Genera*. Cambridge University Press.

Scalzo F, Totis G, Vaglio E, et al. (2021) Experimental study on the high-damping properties of metallic lattice structures obtained from slm. *Precision Engineering* 71: 63–77. https://doi.org/10.1016/j.precisioneng.2021.02.010

Seki Y, Bodde SG and Meyers MA (2010) Toucan and hornbill beaks: a comparative study. *Acta Biomaterialia* 6(2): 331–343. https://doi.org/10.1016/j.actbio.2009.08.026

Shah MU, Usman M, Farooq SH, et al. (2023) Spring-controlled modified tuned liquid column ball damper for vibration mitigation of structures. *Journal of Sound and Vibration* 545: 117443. https://doi.org/10.1016/j.jsv.2022.117443

Sienkiewicz J, Płatek P, Jiang F, et al. (2020) Investigations on the mechanical response of gradient lattice structures manufactured via slm. *Metals* 10(2): 213. https://doi.org/10.3390/met10020213

Syam WP, Jianwei W, Zhao B, et al. (2018) Design and analysis of strut-based lattice structures for vibration isolation. *Precision Engineering* 52: 494–506. https://doi.org/10.1016/j.precisioneng.2017.09.010

Valdevit L, Pantano A, Stone HA, et al. (2006) Optimal active cooling performance of metallic sandwich panels with prismatic cores. *International Journal of Heat and Mass Transfer* 49(21-22): 3819–3830. https://doi.org/10.1016/j.ijheatmasstransfer.2006.03.042

Van der Burg M, Shulmeister V, Van der Geissen E, et al. (1997) On the linear elastic properties of regular and random open-cell foam models. *Journal of Cellular Plastics* 33(1): 31–54. https://doi.org/10.1177/0021955X9703300103

Verbaan CA, Peters GW and Steinbuch M (2017) The advantage of linear viscoelastic material behavior in passive damper design-with application in broad-banded resonance dampers for industrial high-precision motion stages. *Journal of Sound and Vibration* 386: 242–250. https://doi.org/10.1016/j.jsv.2016.05.031

Wang G, Shen L, Zhao J, et al. (2018) Design and compressive behavior of controllable irregular porous scaffolds: based on voronoi-tessellation and for additive manufacturing. *ACS Biomaterials Science & Engineering* 4(2): 719–727. https://doi.org/10.1021/acsbiomaterials.7b00916

Wee KM, Rogers TN, Altan BS, et al. (2005) Engineering and medical applications of diatoms. *Journal of Nanoscience and Nanotechnology* 5(1): 88–91. https://doi.org/10.1166/jnn.2005.020

Yin S, Wu L, Yang J, et al. (2014) Damping and low-velocity impact behavior of filled composite pyramidal lattice structures. *Journal of Composite Materials* 48(15): 1789–1800. https://doi.org/10.1177/0021998313490582

Zheng Z, Yu J and Li J (2005) Dynamic crushing of 2d cellular structures: a finite element study. *International Journal of Impact Engineering* 32(1-4): 650–664. https://doi.org/10.1016/j.ijimpeng.2005.05.007

Zhou S and Bao B (2025) A lever-enhanced tuned inerter damper for controlling vibrations due to rotary unbalance and bounded parametric uncertainty: classic and robust equal-peak optimization. *Journal of Sound and Vibration* 596: 118777. https://doi.org/10.1016/j.jsv.2024.118777

Zhu HX, Hobdell JR and Windle AH (2000) Effects of cell irregularity on the elastic properties of open-cell foams. *Acta Materialia* 48(20): 4893–4900. https://doi.org/10.1016/S1359-6454(00)00282-2

Zhu H, Hobdell J and Windle A (2001) Effects of cell irregularity on the elastic properties of 2d voronoi honeycombs. *Journal of the Mechanics and Physics of Solids* 49(4): 857–870. https://doi.org/10.1016/S0022-5096(00)00046-6

Zhu Y, Guo X, Wang Q, et al. (2024) A lightweight tuned particle damper for low-frequency vibration attenuation. *Journal of Sound and Vibration* 583: 118440. https://doi.org/10.1016/j.jsv.2024.118440